Quantum statistics of light emitted from a pillar microcavity

Timur A. Khudaiberganov[1] · Igor Yu. Chestnov[1,2] · Sergei M. Arakelian[1]

Abstract

A quantum behavior of the light emitted by exciton polaritons excited in a pillar semiconductor microcavity with embedded quantum well is investigated. Considering the bare excitons and photon modes as coupled quantum oscillators allows for an accurate accounting of the nonlinear and dissipative effects. In particular, using the method of the quantum states representation in a quantum phase space via quasiprobability functions (namely, a *P*-function and a Wigner function), we study the impact of the laser and the exciton-photon detuning on the second order correlation function of the emitted photons. We determine the conditions under which the phenomena of bunching, giant bunching, and antibunching of the emitted light emerge. In particular, we predict the effect of a giant bunching for the case of a large exciton to photon population ratio. Within the domain of parameters supporting a bistability regime we demonstrate the effect of bunching of photons.

1 Introduction

Exciton polaritons are mixed quasiparticles arising due to the strong coupling of photonic mode with an exciton resonance. Being initially considered as a fundamental example of composite bosons with small effective mass, which is beneficial for a high-temperature condensation, the exciton polaritons are recognized now to be well suited for realization of the practical devices being competitive with the state of the art optoelectronic and photonic devices. Indeed, the composite nature of exciton polaritons takes advantage of both photonic and excitonic constituents. Namely, polaritons inherit a high mobility and the ease of excitation from photons as well as the strong two-body interactions from excitons. This combination makes polaritonic systems a versatile platform for studying quantum and nonlinear phenomena in strongly coupled light-matter systems.

We consider the exciton polaritons (hereafter polaritons) formed in a pillar microcavity [1]—see the sketch in Fig. 1. The micropillar is characterised by a narrow optical cone. Therefore, in contrast to a planar microcavity, it is capable of supporting a tightly confined condensate whose spatial

degrees of freedom are suppressed. In what follows, we consider "zero-dimensional" polaritons formed in a small micropillar.

The quantum and nonlinear properties of exciton polaritons are of a great interest. When the cavity is driven by the external laser, the nonlinear behavior can be revealed in a bistable optical response [2] of the medium. This phenomenon is classical and can be observed by a hysteresis of the cavity transmission characteristic measured by scanning adiabatically the intensity of the pumping laser. Here, in contrast, we are interested in the quantum manifestations of the bistability effect. In particular, we study the statistics of the light emitted by the microcavity. Note that manifestations of the quantum statistics under the bistabitility conditions were previously observed in the cavity-QED systems [3, 4]. We are aimed at searching of the conditions when the system behavior differs strongly from what the classical description predicts. For example, the influence of a classical noise on the exciton-polariton bistability has already been considered in Ref. [5]. At the same time, in the experimental works [6, 7], a bistable response characterized by the hysteresis loop was observed to be narrower than it was expected in the classical case. Such a squeezing of the bistability loop indicates a significant impact of the quantum noise effects on the polariton behavior.

A general characteristic of the quantum properties of a given system is a second order correlation function $g^{(2)}(\tau) = \frac{\langle a(t)^+ a(t+\tau)^+ a(t) a(t+\tau)\rangle}{\langle a(t)^+ a(t)\rangle^2}$. At zero time-delay $\tau = 0$, it is $g^{(2)}(0) = 1 + \frac{\langle(\Delta n)^2\rangle - \langle n\rangle}{\langle n\rangle^2}$. For example, a dramatic decrease of

✉ Timur A. Khudaiberganov
  thomasheisenberg@mail.ru

1 Department of Physics and Applied Mathematics, Vladimir State University named after A. G. and N. G. Stoletovs, 87 Gorkii st., Vladimir 600000, Russia

2 ITMO University, St. Petersburg 197101, Russia

Fig. 1 A sketch of the micropillar with embedded quantum well supporting formation of zero-dimensional polaritons (purple dot). The arrow illustrates the external laser pump which drives the photonic mode of the cavity
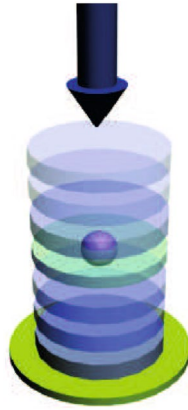
this quantity above threshold can be considered as a fingerprint of Bose condensation in the exciton-polariton system formed in a planar microcavity [8]. The value of the second order correlation function indicates on such quantum phenomena as bunching ($g^{(2)} > 1$) and antibunching ($g^{(2)} < 1$). The effect of antibunching was studied for polaritons formed in a quantum box in the context of so-called polariton blockade [9], when the emission of photons in pairs is suppressed and photons are emitted individually. The second order correlation function of the photons emitted from the micropillar driven by the laser light demonstrates a sharp peak [10] in the phase transition region, while in a planar microcavity this value demonstrates a smooth dependence on the pump power beyond the threshold [8]. The quantum properties of the excitonic component of polariton state were theoretically investigated in Ref. [11]. In particular, the peak of the second order correlation function of excitons was predicted. In this article, we focus on the investigation of the quantum behavior of the photonic mode.

To solve an open quantum nonlinear problem, we use a powerful analytical method of the generalized P-representation [12]. Unlike numerical approaches, this method allows for investigation of the quantum properties in entire region of the quantum phase space. Besides, it contrasts to the linearization [14] and perturbation [15] methods which does not account for the strong quantum fluctuations in the vicinity of the quantum phase transition.

The paper is organized as follows. In Sect. 2 we introduce the Hamiltonian of the system and derive the master equation. Next, we move to the description of this system in a quantum phase space, namely, to the P-representation. We solve the Fokker–Planck equation for the P-function using the method of potential [12] and obtain the first and second order correlation functions [11] of the photons using the governing (slaving) principle. Note that the perturbation theory does not predict the observable peak of the second order correlation function [13] in this case. In Sect. 3, we investigate the effect of quantum fluctuations on the bistability. In Sect. 4, we study the effects of the giant bunching

and antibunching effects in the region of a triple resonance where the exciton, photon and the laser frequencies are close to each other. In Sect. 5, we study non-classic states in the strong pump regime.

2 The model

Polaritons are excited by a coherent laser whose frequency is close both to the photon ω_{ph} and exciton ω_{ex} resonances. The Hamiltonian of two coupled modes in the presence of coherent pumping in the rotating wave approximation [2, 11] reads:

$$
\begin{aligned}
\hat{H}_S =&\, \hbar\Delta_{\mathrm{ph}}\hat{\phi}^+\hat{\phi} - \hbar\Delta_{\mathrm{ex}}\hat{\chi}^+\hat{\chi} \\
&+ \hbar\omega_{\mathrm{R}}\big(\hat{\chi}^+\hat{\phi} + \hat{\phi}^+\hat{\chi}\big) + \hbar\alpha\hat{\chi}^{+2}\hat{\chi}^2 + i\hbar\big(\tilde{E}_{\mathrm{d}}\hat{\phi}^+ - \tilde{E}_{\mathrm{d}}^*\hat{\phi}\big).
\end{aligned}
\tag{1}
$$

Here $\hat{\phi}$ ($\hat{\phi}^+$) and $\hat{\chi}$ ($\hat{\chi}^+$) are annihilation (creation) operators of the photon and the exciton modes, respectively. $\tilde{E}_{\mathrm{d}}$ stands for the strength of the coherent pump driving the cavity mode at the frequency ω_{d}. The value $\Delta_{\mathrm{ph}} = \omega_{\mathrm{ph}} - \omega_{\mathrm{d}}$ stands for the detuning of the photon frequency from the frequency of the pump while $\Delta_{\mathrm{ex}} = \omega_{\mathrm{d}} - \omega_{\mathrm{ex}}$—is the detuning of the excitonic resonance, ω_{R} equals to a half of the Rabi splitting, α—is a coefficient of a Kerr-like nonlinearity which stems from the exciton-exciton scattering.

The polariton condensate under consideration is an open quantum system which is inevitably affected by the presence of noise. We suppose that the micropillar temperature is about several Kelvin. In this case, the thermal noise is weak since the influence of the heat reservoir decreases exponentially with the increase of the ratio $\hbar\omega_{\mathrm{ph,ex}}/k_{\mathrm{B}}T$. In our case $\hbar\omega_{\mathrm{ph,ex}} \gg k_{\mathrm{B}}T$, therefore we neglect by the presence of thermal noise. Also, we exclude the classical fluctuations from the driving laser [5]. Thus we are left with a purely quantum noise whose impact on the system behavior is studied below.

We treat the losses of the exciton-photon system via the Lindblad master equation (in the Born–Markov approximation) for the density operator ρ [11],

$$
\begin{aligned}
\frac{\partial\rho}{\partial t} =&\, \frac{1}{i\hbar}\big[\hat{H}_S, \rho\big] + \gamma_{\mathrm{ph}}\big(2\hat{\phi}\rho\hat{\phi}^+ - \rho\hat{\phi}^+\hat{\phi} - \hat{\phi}^+\hat{\phi}\rho\big) \\
&+ \gamma_{\mathrm{ex}}\big(2\hat{\chi}\rho\hat{\chi}^+ - \rho\hat{\chi}^+\hat{\chi} - \hat{\chi}^+\hat{\chi}\rho\big),
\end{aligned}
\tag{2}
$$

where γ_{ph} and γ_{ex} are the damping rates of photonic and excitonic modes, respectively.

The semiclassical solution of the problem has been described in a number of works [2, 11, 16]. In particular, it predicts the bistable optical response of the microcavity which manifests itself in a hysteretic behavior of the output light intensity [2]—see Fig. 2b. The optical bistability effect occurs within the particular range of the driving field which
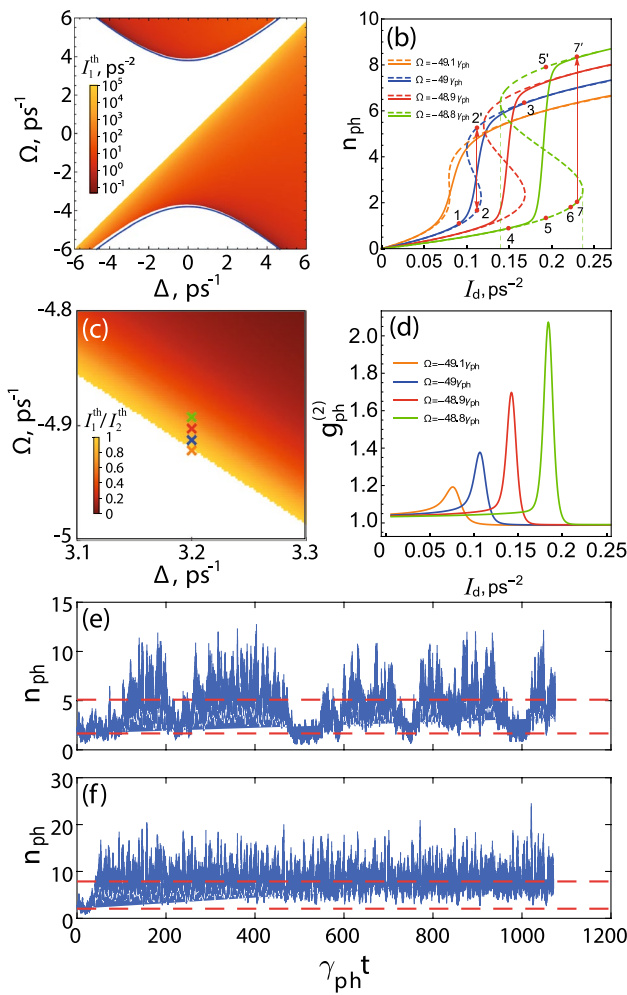
Fig. 2 **a** The bistability map on the (Δ, Ω)-plane. Shaded region corresponds to the existence of bistability. Color of the filling encodes the driving field intensity I_1^{th} corresponding to the left turning point of the $n_{ph}(I_d)$ curve, see panel (**b**). **b** The semiclassical population of the photonic mode n_{ph} and the analytical quantum solution (4) for $\langle \phi^+ \phi \rangle$ at $\Delta = 32\gamma_{ph}$, $\Omega = -49.2\gamma_{ph}$ (orange line), $\Omega = -49.1\gamma_{ph}$ (blue line), $\Omega = -49\gamma_{ph}$ (red line), $\Omega = -48.9\gamma_{ph}$ (green line)—see the color crosses on the panel (**c**). **c** the ratio of the driving intensities I_1^{th} and I_2^{th} corresponding to the left and the right turning points of the bistability loop. **d** The $g_{ph}^{(2)}(I_d)$-dependence at the same parameters as in panel (**b**). The other parameters are $\alpha = 0.015\gamma_{ph}$, $\omega_R = 25\gamma_{ph}$, $\gamma_{ex} = 0.01$ ps^{-1} and $\gamma_{ph} = 0.1$ ps^{-1}. **e**, **f** Numerical simulations of the stochastic dynamics of the photon number predicted by the equations (A.4). The initial state corresponds (**e**) to the point 2 on the panel (**b**) and (**f**) to the point 7

is determined by a competition between the losses and the positive nonlinear feedback of microcavity excitons [5].

The steady state quantum solution of the master equation (2) is obtained analytically using the *P*-function approach—see Appendix 1. In what follows we assume that the quantum fluctuations of the photonic mode are governed to the quantum fluctuations of excitons [17, 18]

according to the Haken's slaving principle. Thus using the first equation from (A.4), in the steady state regime we obtain the following relation between the amplitudes of the photon and the exciton fields:

$$\phi = \frac{\tilde{E}_d(\gamma_{ph} - i\Delta_{ph})}{\left(\Delta_{ph}^2 + \gamma_{ph}^2\right)} - \frac{\omega_R(i\gamma_{ph} + \Delta_{ph})}{\left(\Delta_{ph}^2 + \gamma_{ph}^2\right)}\chi. \tag{3}$$

In this case a first order correlation function of photons, which is equivalent to a quantum average value of the photon number, is defined as

$$\langle \phi^+ \phi \rangle = \frac{I_d + \omega_R^2 G^{(11)} + 2\omega_R \text{Im}\left(\tilde{E}_d G^{(10)}\right)}{\left(\Delta_{ph}^2 + \gamma_{ph}^2\right)}. \tag{4}$$

Here $G^{(ij)} = \left\langle \left(\chi^+\right)^i \chi^j \right\rangle$—is a correlation function of the exciton mode, see Appendix 1. The value $I_d = |E_d|^2$ is proportional to the intensity of the laser pump.

We characterize the quantum properties of the emitted light with the second order correlation function $g_{ph}^{(2)} = \frac{\langle \phi^{+2} \phi^2 \rangle}{\langle \phi^+ \phi \rangle^2}$. From (3) with the use of Eq. (10) given in the Appendix 1 one obtains:

$$g_{ph}^2(0)$$

$$= \frac{I_d^2 - \omega_R^2(\tilde{E}_d^2 G^{(20)} + \tilde{E}_d^{*2} G^{(02)}) + 2i\omega_R I_d(\tilde{E}_d G^{(10)} - \tilde{E}_d^* G^{(01)})}{I_d + \omega_R^2 G^{(11)} + i\sqrt{I_d}\omega_R\left(G^{(10)} - G^{(01)}\right)}$$

$$\frac{[2i\omega_R^3(\tilde{E}_d G^{(21)} - \tilde{E}_d^* G^{(12)}) + 4\omega_R^2 I_d G^{(11)} + \omega_R^4 G^{(22)}}{I_d + \omega_R^2 G^{(11)} + i\omega_R\left(\tilde{E}_d G^{(10)} - \tilde{E}_d^* G^{(01)}\right)}. \tag{5}$$

3 Polariton bistability in the presence of quantum fluctuations

For the given problem (1), one can obtain the steady state solution in the mean field approximation. It implies averaging quantum operators $O_{mf} = \langle \hat{O} \rangle = \text{Tr}(\rho\hat{O})$ and factorization of the quantum averages as $\langle \hat{\chi}^+ \hat{\chi}\hat{\chi} \rangle \rightarrow |\chi_{mf}|^2 \chi_{mf}$. In this case the bistability phenomenon is manifested in the typical *S*-shape intensity-dependence of the photon mode population, see the dashed curves in Fig. 2b. The region where the solution is bistable, is displayed on the parameter plane (Δ, Ω), Fig. 2a. Here $\Delta = \frac{\omega_{ph} - \omega_{ex}}{2}$ and $\Omega = \omega_d - (\omega_{ph} + \omega_{ex})/2$ is a detuning of the driving field from the central frequency between the exciton and the photon resonances. The false colors in Fig. 2a correspond to the critical intensity of the driving field above which the single-valued solution is superposed by a bistable one. This value is refereed to as a bistability threshold. There are two

domains of bistability: The upper and the lower one. On the energy scale, both domains are located above the relevant polariton branches $\Delta_{\text{LP,UP}} = \pm\sqrt{\omega_R^2 + \Delta^2}$ shown with the blue lines. In particular, the regions of bistability are shifted upwards in frequency on the value which is determined by the level of losses [2].

The upper and lower segments of the bistability curve shown in Fig. 2b are stable in the mean field approximation. It means that the polariton mode excited in these configurations live infinitely long. However in the presence of a sufficient external noise the stochastic switching between bistable states becomes possible [19]. The problem of stochastic switching in the exciton-polariton system has already been considered in the context of a dissipative phase transition [7]. A study of the micropillar radiation demonstrated the stochastic switching between the bistable states [7, 10]. Besides, the non-classical behavior was discovered in the quantum statistics of the micropillar radiation [7]. The early theoretical works [7, 10, 19] which address this question used a truncated lower polariton branch approximation [2]. It means that it took into account only the lower polariton state neglecting by all the other terms which appear in the Hamiltonian (1) rewritten in the polariton basis. This approximation is valid when the pump frequency is tuned close to the lower polariton branch resonance. However, in the general case of arbitrary driving frequency, one needs to consider the interaction with both the upper and lower polaritons. In contrast to the previous studies, here we consider a complete model operating in the exciton-photon basis using the slaving principle introduced by Haken [17]. This approach allows for expanding of the parameters region covered by the quantum nonlinear effects caused by the bistability phenomenon.

As opposite to the mean-field solution which predicts two stable stationary states within the bistability region, the quantum approach always yields [12] a single-valued solution (4), see the solid curve in Fig. 2b. However because of the intrinsic quantum noise, the bistable behavior still can be observed within the quantum approach by the presence of the hysteresis loop. The quantum approach treats the upper and lower states of the classical bistability curve as the metastable ones. Whether the system jumps between the metastable states or not depends on the time spent in the initial state. Therefore, if one scans the driving intensity up and down, the classical hysteresis loop is revealed only in the case of quasi-adiabatic variation of the pump power. At a finite scanning velocity the dynamical hysteresis loop becomes narrower as it was demonstrated in [6]. The loop width depends on the pumping rate variation rate and on the lifetime of metastable states [6]. Which is why the resulted $n_{\text{ph}}(I_d)$-dependence is called a dynamic hysteresis loop.

The dynamics of the stochastic jumps can be described with the use of the stochastic differential equations (A.4) for the quantum variables (the commutative c-numbers ϕ, ϕ^+, χ and χ^+) [12, 13],—see Eq. (A.4). These equations include the diffusion and drift terms inherited from the Fokker–Planck equation (8). The details are given in the Appendix 1.

The solid curves in Fig. 2b show predictions of the quantum solution for various laser detunings (indicated by the crosses in Fig. 2c). Our analysis reveals the presence of quantum jumps between two metastable states at the pump intensity corresponding to the fast variation of the photon number predicted by the quantum solution. In this region, the mean number of photons n_{ph} rapidly grows from the lower to the upper bistable state. The stochastic dynamics demonstrating quantum jumps is shown in Fig. 2e. The parameters of the system correspond to the blue curve in Fig. 2b. The metastable states are indicated by points 2 and 2′ connected with the red arrow. The stable states appear in the region where the quantum solution is close to the semiclassical one (points 1 and 3 on the blue curve and point 4 on the green curve). Note that for the case of a wide bistability loop, there is typically only one stable branch of the classical solution, while the states on the opposite branch of the loop are metastable. This is the case of the point 7 which corresponds to the metastable state located at the lower branch of the green curve. The stochastic dynamics of the system initially excited in the state 7, as it is shown in Fig. 2f, demonstrates an irreversible jump to the state 7′ corresponding to stable upper state.

Thus, we distinguish two dynamical regimes. In the first regime, the frequent jumps occur as it is shown in Fig. 2e. In Fig. 2b this regime corresponds to the orange and the blue curves. Since this behavior is caused by the quantum noise, this regime is referred to as a quantum one. In the bistability diagram, this regime is realised in the vicinity of the boundary of the bistability existence domain, see Fig. 2c. In this region, the pump intensities corresponding to the turning points of the classical S-shaped bistability curve are close to each other. The second case is characterized by the narrow range of the pump intensities at which the quantum jumps occur. Within this range, the mean photon number (4) grows steeply. On the contrary, the region of the metastable solutions characterized by a single jump behavior shown in Fig. 2f is typically much wider, see the red and the green curves in Fig. 2b. The second regime occurs outside of the boundary of the bistability existence domain (see Fig. 2c), where the classical bistability curve is wide. Adopting the terminology from [20] we call this case a quasiadiabatic regime implying quasi-equilibrium of the system. In Ref. [20], a similar regime was considered in the context of the dissipative phase transition which is manifested by
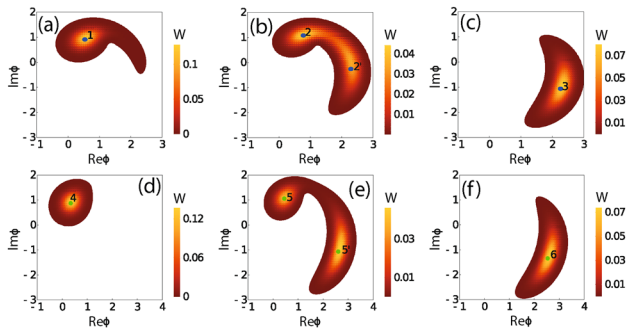
Fig. 3 The Wigner function distribution $W(\mathrm{Re}(\phi), \mathrm{Im}(\phi))$ characterizing the photonic fraction. Panels (a), (b) and (c) correspond to different positions on the blue curve shown in Fig. 2b indicated by the points 1, 2 and 3 respectively. The detunings are $\Omega = -49.1\gamma_{\mathrm{ph}}$ and $\Delta = -32\gamma_{\mathrm{ph}}$. Panels (d), (e) and (f) correspond to the points 4, 5 and 6 on the green curve, respectively. The detunings are $\Omega = -48.9\gamma_{\mathrm{ph}}$, $\Delta = -32\gamma_{\mathrm{ph}}$. The other parameters are the same as in Fig. 2

closing of the Liouvillian gap in the thermodynamic limit (when the number of particles tends to infinity). However, in our case, a similar regime occurs at the small population of the state.

the differences between two regimes can be clearly illustrated with the use of the Wigner function representation, see Fig. 3. The coexistence of two metastable states is indicated by a bimodal structure [21] of the Wigner function illustrated in Fig. 3b, e. Note that when a single stable state exists, the Wigner function is characterized by a single peak, see the panels (a), (c), (d) and (f) corresponding to the points 1, 3, 4 and 6 in Fig. 2b, respectively. For the quantum regime, in the particular case corresponding to the recurrent jumps between the points 2 and 2′ in Fig. 2b, one can observe a pronounced overlap of the quasi-probability distributions corresponding to two bistable states, see Fig. 3b. On the contrary, for the quasiadiabatic case, corresponding to the points 5 and 5′ in Fig. 2b the quasiprobability is localized in the two regions with almost no overlap between them, see Fig. 2e.

The quantum behavior of the photonic mode in the bistable regime is reflected in its statistics. In the region where the quantum average photon number grows steeply, we observe a peak of the second order correlation function $g_{\mathrm{ph}}^{(2)}$, see Fig. 2d, which corresponds to the bunching of the photons emitted by the micropillar. Figure 2d shows the second order correlation functions of photons for various laser detunings Ω corresponding to the solutions shown in Fig. 2b. We can see an increase of the peak amplitude accompanied by the decrease of its width as the laser intensity growth. In this case, the width of the peak of the $g_{\mathrm{ph}}^{(2)}$ function is comparable with the width of $n_{\mathrm{ph}}(I_{\mathrm{d}})$-dependence predicted by the quantum solution.
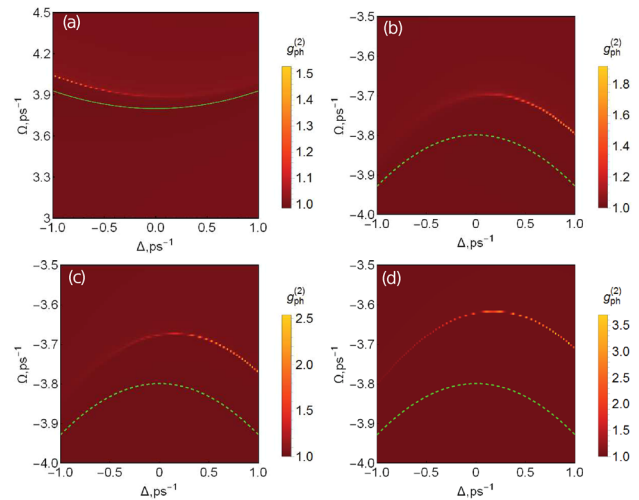

Fig. 4 The maps of the second order correlation function of photons in the vicinity of the upper polariton branch (**a**) and of the lower polariton branch (**b–d**). The polariton frequencies are indicated by the green dotted lines. The driving intensity is **a** $I_{\mathrm{d}}/\gamma_{\mathrm{ph}}^2 = 100$, **b** $I_{\mathrm{d}}/\gamma_{\mathrm{ph}}^2 = 70$, **c** $I_{\mathrm{d}}/\gamma_{\mathrm{ph}}^2 = 100$ and **d** $I_{\mathrm{d}}/\gamma_{\mathrm{ph}}^2 = 200$

Figure 4 shows a map of the second order correlation function on the (Ω, Δ) parameter space for various driving intensities: (b) $I_{\mathrm{d}}/\gamma_{\mathrm{ph}}^2 = 70$, (a), (c) $I_{\mathrm{d}}/\gamma_{\mathrm{ph}}^2 = 100$, and (d) $I_{\mathrm{d}}/\gamma_{\mathrm{ph}}^2 = 200$. Panels (b–d) show the region in the vicinity of the resonance of the lower polariton (LP) branch (the green dotted curves), while panel (a) is focused on the upper polariton (UP) branch. One can see a bright narrow band which corresponds to the peaks of the $g_{\mathrm{ph}}^{(2)}$ function while the background value is $g_{\mathrm{ph}}^{(2)} = 1$. This band follows position of the LP branch. Note that the narrow band of the bunching states as well as the peak magnitude of the $g_{\mathrm{ph}}^{(2)}$ shifts towards larger driving detunings Ω as the pump intensity increases. Besides, the peak of the second order correlation function is more pronounced for a positive detuning, $\Delta > 0$. This is because the quantum fluctuations of the lower polaritons play a dominant role near the LP resonance (in contrast to the fluctuations of the upper polaritons which are suppressed in this domain). The fluctuations are more pronounced for the positive detunings since in this region the excitonic fraction of the LP state dominates over the photonic fraction. It is reflected in the value of the Hopfield coefficients $C_{\mathrm{ex}} = \sqrt{\frac{1}{2}\left(1 - \frac{\Delta}{\sqrt{\Delta^2 + \omega_{\mathrm{R}}^2}}\right)}$ and $C_{\mathrm{ph}} = \sqrt{\frac{1}{2}\left(1 + \frac{\Delta}{\sqrt{\Delta^2 + \omega_{\mathrm{R}}^2}}\right)}$ which determine the exciton and photon fractions of the polariton state, respectively. In particular, for the positive detuning, $C_{\mathrm{ex}} > C_{\mathrm{ph}}$.

Summarizing this section, we emphasize a crucial role of the quantum noise in the optical bistability phenomenon in the pillar microcavities. The noise-induced quantum jumps between metastable states wash out the hysteresis loop and lead to the non-classical statistics of the emitted light. However in practice, the stochastic behavior of optical photons is observable only in the vicinity of the bistability threshold, i.e. where the classical hysteresis loop is narrow. For the wide loops, the time spent by the system in the metastable state quickly grows with the increase of the loop width and can become impractically long as it was discussed in Ref. [20]. The non-classical statistics of the emitted light can be detected within a wide range of the laser driving detunings in the vicinity of both lower and upper polariton resonances. However, the range where the noise-induced behavior takes place is not limited solely to the domain of bistability. In the following section we demonstrate the phenomena of photon antibunching and giant bunching which occur far from the bistability existence domain.

4 Triple resonance region

In this section, we focus on the parameter region close to the triple resonance between the exciton, photon and the pumping laser frequencies, $\Omega = 0$ and $\Delta = 0$. In this case we
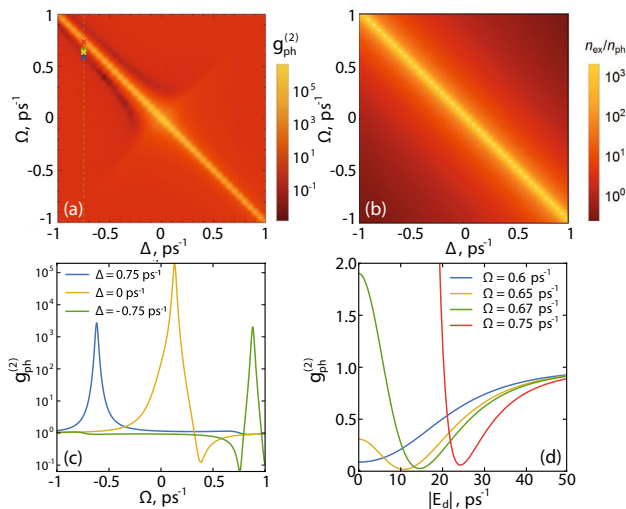

Fig. 5 **a** The zero-delay second order correlation function of photons $g_{ph}^{(2)}(0)$ for various values of driving detuning Ω and exciton-photon detuning Δ. **b** The ratio between populations of the excitonic and photonic modes n_{ex}/n_{ph} in the same parameter plane as in the panel (**a**); **c** the dependence of $g_{ph}^{(2)}(0)$ on the driving detuning Ω for the fixed values of the exciton-photon detuning, shown by the vertical dot-dashed lines in the panel (**a**), $\Delta = -7.5\gamma_{ph}$ (green line), $\Delta = 0$ (yellow line), and $\Delta = 7.5\gamma_{ph}$ (blue line). **d** The dependence of $g_{ph}^{(2)}(0)$ on the driving amplitude $|E_d|$ at $\Delta = -7.5\gamma_{ph}$, and at the fixed values of the laser detuning [color crosses on the panel (**a**)], $\Omega = 6\gamma_{ph}$ (blue line), $\Omega = 6.5\gamma_{ph}$ (yellow line), $\Omega = 6.7\gamma_{ph}$ (green line), and $\Omega = 7.5\gamma_{ph}$ (red line)

observed the bunching, giant bunching and the antibunching phenomena. The (Ω, Δ) – map of the second order correlation function $g_{ph}^{(2)}(0)$ in the vicinity of the triple resonance is shown in Fig. 5a. One can see a domain of the bright false-color corresponding to the effect of the giant bunching, $g_{ph}^{(2)} \gg 1$, along to the line $\Omega \approx -\Delta$. Note that this condition corresponds to the excitonic resonance $\omega_d \approx \omega_{ex}$. This behavior should be attributed to the imbalance of the photon and the exciton populations. In particular, in the region of the giant bunching, the exciton population dominates over the cavity mode occupation $n_{ex}/n_{ph} \gg 1$ as it is shown in Fig. 5b. Therefore, the weak quantum fluctuations of the exciton mode cause strong fluctuations of the photon mode according to the slaving principle [18], see Eq. (3). This is illustrated in Fig. 5b which demonstrates the map of the n_{ex}/n_{ph} ratio. The maximum in Fig. 5b follows the region of the giant photon bunching effect. Note, that for the considered parameters the value of $g_{ph}^{(2)}(0)$ in the giant bunching regime reaches 10^5 as it is illustrated in Fig. 5c demonstrating a cross-sections of the map shown in Fig. 5a for the fixed values of the exciton-photon detuning.

At the negative detuning Δ, the effect of the giant bunching adjoins the region with $g_{ph}^{(2)} < 1$, where the cavity photons are in the antibunched state, cf. with [22]. This regime is realised at the negative exciton-photon detuning Δ while the pump frequency ω_d is weakly detuned from the excitonic resonance ω_{ex}, see Fig. 5a. The transition from the bunching to the antibunching statistics with the variation of the driving laser frequency is clearly seen in Fig. 5c. The $g_{ph}^{(2)}(|E_d|)$ -dependence is shown in Fig. 5d at different exciton-photon detunings: $\Omega = 6\gamma_{ph}$, $\Omega = 6.5\gamma_{ph}$, $\Omega = 6.7\gamma_{ph}$, and $\Omega = 7.5\gamma_{ph}$. The antibunching is typically observed at the moderate driving strength while in the limit of strong driving the cavity field approaches coherent statistics, $g_{ph}^{(2)} \approx 1$.

5 Non-classic states

The effect of antibunching was studied for polaritons formed in a quantum box in the context of so-called polariton blockade [9]. In particular, the antibunching phenomenon was predicted to occur only at sufficiently large nonlinear interaction strength which requires a microcavity with a very small mode volume [9]. However, reducing the mode volume down to a subwavelength size has a drawback of the degradation of the microcavity quality factor which corresponds to the increase of the cavity mode dissipation rate. Here, we demonstrate that the antibunching effect can be obtained with the small values of the nonlinear interaction strength which are achievable in the state of the art pillars microcavities. This is demonstrated in Fig. 6a which shows
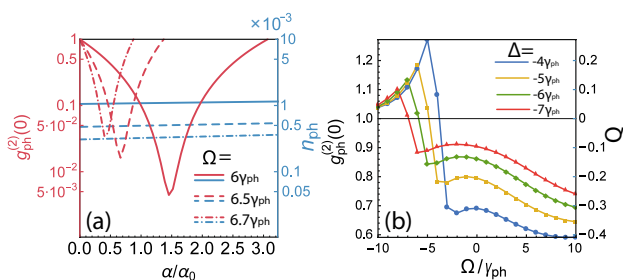
Fig. 6 **a** The second order correlation function of photons versus the nonlinearity strength α at $\Delta = -7.5\gamma_{ph}$ and different values of Ω shown in the inset. **b** The second order correlation function of photons and the Mandel parameter Q versus the laser detuning Ω. The average photon number is taken as $\langle \phi^+\phi \rangle = 1$ at every point. The parameters are $\Delta = -4\gamma_{ph}$—the blue line, $\Delta = -5\gamma_{ph}$—the yellow line, $\Delta = -6\gamma_{ph}$—the green line, $\Delta = -7\gamma_{ph}$—the red line

the second order correlation function of photons for different values of the nonlinear interaction strength normalized to $\alpha_0 = 0.015\gamma_{ph}$ which corresponds to the value used for the rest of the calculations in the paper. The antibunching of the cavity photons can be observed even at weak nonlinearities.

The strong antibunching can serve as a manifestation of the quantum blockade phenomenon. This effect can facilitate creation of single photon sources. That is why the relevant phenomenon of the polariton blockade is of a great interest now [23]. Another important question is whether the photonic field emitted by the microcavity reflects the statistic of the intracavity polaritons. To answer this question, we address the statistical properties of the second constituent of polaritons—the quantum well excitons. The effects of antibunching can be also observed for the excitonic mode. However, in contrast to the case of photons, the exciton antibunching is weak due to the large number of excitons in the vicinity of the triple resonance. In fact, the $g_{ex}^{(2)}$ map follows that of the photon field though the peak and the minimal values of the correlation function are much lower. In the antibunching region, $g_{ex}^{(2)}$ is typically a little less than one. The quantum statistics of lower branch polaritons combines the statistics of photons and excitons. However due to the domination of the exciton field it is mostly governed by the exciton statistics. Indeed, one can easily check that the condition $g_{LP}^{(2)} \geq (g_{ph}^{(2)} + g_{ex}^{(2)})/2$ holds in the region close to the triple resonance. It means that polaritons do not exhibit a noticeable antibunching effect in contrast to photons. Therefore, it is necessary to emphasis that the quantum statistics of polaritons does not have to coincide with the statistics of the microcavity radiation. When the microcavity emits light, polariton state collapses to the photonic state inheriting the energy and momentum from the polariton. However, the statistics of the emitted photonic field can be completely different.

The antibunching effect leads to the anticorrelation of the photon pairs, which typically results in a sub-Poissonian

distribution of the number of photons. The characteristic of the deviation of the statistics from the Poissonian one is the Mandel parameter [24]:

$$Q = \frac{\langle \Delta n^2 \rangle}{\langle n \rangle} - 1. \tag{6}$$

At $Q = 0$ the photon-number statistics is Poissonian. One can connect the Mandel parameter with the second order correlation function $g_{ph}^2(0)$ as

$$Q = \langle n_{ph} \rangle (g_{ph}^{(2)}(0) - 1). \tag{7}$$

The antibunching effect demonstrated in Fig. 6a occurs at the small average number of photons, see the values corresponding to the right vertical axis. In these particular cases, $Q \approx 0$ according to Eq. (7) which means that the statistics of photons is just slightly sub-Poissonian, $Q < 0$. We then consider the case of the larger population of the photonic mode. In particular, we fix the average number of photons at the level of $\langle n_{ph} \rangle = 1$ by tuning the intensity of the pump at each value of the varying detuning Ω. The corresponding $g_{ph}^2(\Omega)$ -dependences are shown in Fig. 6b. At $\Omega > 0$ the antibunching effect corresponds to the statistic of photons being close to the sub-Poissonian distribution since $Q < 0$, see the right vertical axis in the Fig. 6b.

6 Conclusion

The quantum behavior of exciton polaritons formed in the micropillar cavity was studied in detail. The quantum solution obtained with the use of the quantum phase space method allows for calculation of the quantum statistical averages such as $g_{ph}^{(2)}$-parameter. The effect of quantum fluctuations on bistability was analyzed. We observe the presence of the quantum jumps between the states corresponding to the upper and lower branches of the bistability curve. Previously, these stochastic jumps between bistable states were observed experimentally [5, 10, 25]. We distinguish between several regimes in the bistablity region: (1) a quantum regime with nontrivial quantum behavior and smooth transition between the bistable states; (2) the quasiadiabatic case which is characterised by the presence of metastable states and a sharp transition between them. The peak of the second order correlation function corresponding to the nontrivial quantum statistics of the micropillar radiation was observed. It should be noted that the approaches developed in Refs. [6, 7, 19] used a single-mode approximation that takes into account only the lower polariton branch, when the pump frequency is tuned close to the resonance with the frequency of the LP branch. The contribution of the upper polariton the branch was neglected. Our work expands the range of system

parameters where the effect of the quantum noise on the statistical properties of the exciton-photon system can be analyzed.

In the region of the triple resonance, we discovered the non-classical behavior of photons, namely, the antibunching and the giant bunching phenomena. Moreover, the antibunching effect is observed even at weak nonlinearity. These results paves the way to the implementation of polariton

$$P_{\mathrm{ss}}\left(\chi, \chi^{+}\right) = N \chi^{-2-i\frac{\gamma}{\alpha}} \chi^{+-2+i\frac{\gamma^{*}}{\alpha}} \exp\left(-\sigma \tilde{E}_{\mathrm{d}} \frac{1}{\chi} - \sigma^{*} \tilde{E}_{\mathrm{d}}^{*} \frac{1}{\chi^{+}} + 2\chi \chi^{+}\right),$$
$$(9)$$

where $\gamma = \gamma_{\mathrm{ex}} + \frac{\omega_{\mathrm{R}}^{2}\gamma_{\mathrm{ph}}}{\gamma_{\mathrm{ph}}^{2}+\Delta_{\mathrm{ph}}^{2}} - i\left(\Delta_{\mathrm{ex}} + \frac{\Delta_{\mathrm{ph}}\omega_{\mathrm{R}}^{2}}{\gamma_{\mathrm{ph}}^{2}+\Delta_{\mathrm{ph}}^{2}}\right), \sigma = \omega_{\mathrm{R}} \frac{\gamma_{\mathrm{ph}}-i\Delta_{\mathrm{ph}}}{\alpha\left(\gamma_{\mathrm{ph}}^{2}+\Delta_{\mathrm{ph}}^{2}\right)}$ and N—is a normalization constant.

We use solution (9) to calculate the correlation functions of any order for excitons:

$$G^{(\mathrm{mn})} = \left\langle \left(\chi^{+}\right)^{\mathrm{m}} \chi^{\mathrm{n}}\right\rangle = \int \chi^{+m} \chi^{n} P_{\mathrm{ss}} d\mu$$

$$= (-1)^{n+m} \frac{\left(\sigma\tilde{E}_{\mathrm{d}}\right)^{\mathrm{n}}\left(\sigma^{*}\tilde{E}_{\mathrm{d}}^{*}\right)^{\mathrm{m}} \Gamma\left(i\gamma^{*}/\alpha\right)\Gamma\left(-i\gamma/\alpha\right)}{\Gamma\left(\mathrm{m}+i\gamma^{*}/\alpha\right)\Gamma\left(\mathrm{n}-i\gamma/\alpha\right)} \frac{{}_{0}\mathrm{F}_{2}\left(\mathrm{m}+i\gamma^{*}/\alpha, \mathrm{n}-i\gamma/\alpha, 2|\sigma|^{2}|\tilde{E}_{\mathrm{d}}|^{2}\right)}{{}_{0}\mathrm{F}_{2}\left(i\gamma^{*}/\alpha, -i\gamma/\alpha, 2|\sigma|^{2}|\tilde{E}_{\mathrm{d}}|^{2}\right)}, d$$
$$(10)$$

microcavities for various quantum applications. For example, for the creation of a polariton logic elements (such as polariton trigger proposed in Ref. [26]) or qubits operating under bistablity conditions. The recent experimental studies [27] demonstrated the need of using the medium with relatively strong interparticle interactions for the realization of a strong antibunching with semiconductor microcavities. In our case, the similar effect arises due to the fact that the weak quantum noise of the exciton mode induces strongly pronounced quantum effects in the photon mode according to the slaving principle (3). That is why the effects of strong antibunching appear at the relatively low values of nonlinearity. Note, that the considered problem represents an example of the general system of two strongly coupled dissipative oscillators. Hence our results can be applied to the various experimental setups both in polaritonics and condensed matter physics.

Appendix 1: Derivation of basic equations based on the P-representation method

Using the generalized *P*-representation and using the *c*-numbers instead of operators we turn from master equation (2) to the Fokker–Planck equation for the *P*-function [12]:

$$\frac{\partial P}{\partial t} = \left[-\frac{\partial}{\partial \phi}\left(-\left(i\Delta_{\mathrm{ph}} + \gamma_{\mathrm{ph}}\right)\phi + \tilde{E}_{\mathrm{d}} - i\omega_{\mathrm{R}}\chi\right) \right.$$
$$\left. -\frac{\partial}{\partial \chi}\left(-\left(-i\Delta_{\mathrm{ex}} + \gamma_{\mathrm{ex}}\right)\chi - i\omega_{\mathrm{R}}\phi - 2i\alpha\chi^{+}\chi^{2}\right) \right. \quad (8)$$
$$\left. +\frac{\partial^{2}}{\partial\chi^{2}}\left(-i\alpha\chi^{2}\right) + \mathrm{h.c.}\right]P,$$

where χ and ϕ—are *c*-numbers. A solution of the Fokker–Planck equation (8) is obtained by the method of potentials in the adiabatic limit [12]:

where Γ is a gamma function and ${}_{0}\mathrm{F}_{2}$ is a hypergeometric function.

The stochastic differential equations can be obtained in the Ito calculus by converting the Fokker–Planck equation (8) into the Ito form [12]:

$$\begin{cases} \frac{\partial}{\partial t}\phi = -\left(i\Delta_{\mathrm{ph}} + \gamma_{\mathrm{ph}}\right)\phi + \tilde{E}_{\mathrm{d}} - i\omega_{\mathrm{R}}\chi, \\ \frac{\partial}{\partial t}\phi^{+} = -\left(-i\Delta_{\mathrm{ph}} + \gamma_{\mathrm{ph}}\right)\phi^{+} + \tilde{E}_{\mathrm{d}}^{*} + i\omega_{\mathrm{R}}\chi^{+}, \\ \frac{\partial}{\partial t}\chi = -\left(-i\Delta_{\mathrm{ex}} + \gamma_{\mathrm{ex}}\right)\chi - i\omega_{\mathrm{R}}\phi - 2i\alpha\chi^{+}\chi^{2} + (1-i)\sqrt{\alpha}\chi\xi(t), \\ \frac{\partial}{\partial t}\chi^{+} = -\left(i\Delta_{\mathrm{ex}} + \gamma_{\mathrm{ex}}\right)\chi^{+} + i\omega_{\mathrm{R}}\phi^{+} + 2i\alpha\chi^{+2}\chi + (1+i)\sqrt{\alpha}\chi^{+}\xi^{+}(t), \end{cases}$$
$$(11)$$

where $\xi(t)$ is an independent stochastic function, whose correlation functions satisfy the following relations: $\langle\xi(t)\rangle = 0$, $\langle\xi^{+}(t)\rangle = 0$, $\langle\xi(t)\xi^{+}(t')\rangle = \delta(t-t')$.

Appendix 2: Derivation of the Wigner function

We use the Wigner function for a visual presentation of the statistical properties of the exciton-polariton system based on the steady-state solution for the *P*-function (9). The Wigner function one can be expressed in terms of the *P*-representation as follow [28]:

$$W(\chi) = \frac{2}{\pi}e^{-2|\chi|^{2}} \int_{C_{x}}\int_{C_{x^{+}}} P_{\mathrm{ss}}\left(x, x^{+}\right) \exp\left(2\chi^{*}x + 2\chi x^{+} - 2x^{+}x\right)dx^{+}dx.$$
$$(12)$$

Then substituting (9) in (12), changing variables in the integral as $x \to -E_{\mathrm{d}}\sigma/t$ and using the Schläfli's integral [29]

$$J_{\nu}(z) = \frac{(z/2)^{\nu}}{2\pi i}\int_{C} t^{-\nu-1}\exp\left[t - \frac{z^{2}}{4t}\right]dt, \quad (13)$$

we obtain the following relation for the excitonic Wigner function:

$$W(\chi) = N' e^{-2|\chi|^2} \left| \frac{J_{-i\frac{\gamma}{\alpha}-1}\left(\sqrt{8\tilde{E}_\mathrm{d}\sigma\chi^*}\right)}{(\chi^*)^{-\left(i\frac{\gamma}{\alpha}+1\right)/2}} \right|^2, \tag{14}$$

where N' is a normalization constant, defined by the following expression:

$$N' = \frac{2}{\pi \left|(2\tilde{E}_\mathrm{d}\sigma)^{-i\frac{\gamma}{\alpha}-1}\right|} \frac{\Gamma\left(-i\frac{\gamma}{\alpha}\right)\Gamma\left(i\frac{\gamma^*}{\alpha}\right)}{{}_0\mathrm{F}_2\left(i\gamma^*/\alpha, -i\gamma/\alpha, 2|\sigma\tilde{E}_\mathrm{d}|^2\right)}. \tag{15}$$

Here we use the following expansion of the power series of the Bessel function [30]

$$J_\nu(\sqrt{t}) = \left(\frac{t}{4}\right)^{\nu/2} \sum_{k=0}^{\infty} \frac{(-1)^k (t/4)^k}{k!\,\Gamma(k+\nu+1)}. \tag{16}$$

According to (14) the Wigner function is always positive and equals the squared modulus of the Bessel function with the complex index $-i\gamma/\alpha - 1$. The Wigner function of photons is obtained from the governing principle (3):

$$W(\phi) = N'' \exp\left(-2\frac{\left(\gamma_\mathrm{ph}\mathrm{Im}(\phi)+\Delta_\mathrm{ph}\mathrm{Re}(\phi)\right)^2 + \left(\gamma_\mathrm{ph}\mathrm{Re}(\phi)-\Delta_\mathrm{ph}\mathrm{Im}(\phi)-\tilde{E}_\mathrm{d}\right)^2}{\omega_\mathrm{R}^2}\right)$$
$$\left| \frac{J_{-i\frac{\gamma}{\alpha}-1}\left(\sqrt{8\tilde{E}_\mathrm{d}\sigma\frac{\left(i\tilde{E}_\mathrm{d}+\phi^*\left(\Delta_\mathrm{ph}-i\gamma_\mathrm{ph}\right)\right)}{\omega_\mathrm{R}}}\right)}{\left(\frac{\left(i\tilde{E}_\mathrm{d}+\phi^*\left(\Delta_\mathrm{ph}-i\gamma_\mathrm{ph}\right)\right)}{\omega_\mathrm{R}}\right)^{\left(-i\frac{\gamma}{\alpha}-1\right)/2}} \right|^2, \tag{17}$$

where we introduced new normalized constant $N'' = \frac{\omega_\mathrm{R}^2}{\Delta_\mathrm{ph}^2+\gamma_\mathrm{ph}^2} N'$.

Author Contributions TAK has carried out the analytical and numerical calculations. TAK and IYuC analysed and interpreted the obtained results and prepared the main text of the paper. All the authors contributed to the writing of the final form of the manuscript.

References

1. J.M. Gérard, D. Barrier, J.Y. Marzin et al., Appl. Phys. Lett. **69**, 449 (1996). https://doi.org/10.1063/1.118135
2. A. Baas, J. Karr, H. Eleuch and E. Giacobino, Phys. Rev. A **69**, 023809 (2004). https://doi.org/10.1103/physreva.69.023809
3. W. Choi, J.-H. Lee, K. An et al., Phys. Rev. Lett. **96**, 093603 (2006). https://doi.org/10.1103/PhysRevLett.96.093603
4. B. Ann, Y. Song, J. Kim et al., Sci. Rep. **9**, 17110 (2019). https://doi.org/10.1038/s41598-019-53525-3
5. H. Abbaspour, G. Sallen, S. Trebaol et al., Phys. Rev. B **92**, 165303 (2015). https://doi.org/10.1103/physrevb.92.165303
6. S.R.K. Rodriguez, W. Casteels, F. Storme et al., Phys. Rev. Lett. **118**, 247402 (2017). https://doi.org/10.1103/PhysRevLett.118.247402
7. T. Fink, A. Schade, S. Höfling et al., Nat. Phys. **14**, 365–369 (2017). https://doi.org/10.1038/s41567-017-0020-9
8. H. Deng, G. Weihs, C. Santori et al., Science **298**, 199–202 (2002). https://doi.org/10.1126/science.1074464
9. A. Verger, C. Ciuti, I. Carusotto, Phys. Rev. B **73**, 193306193306 (2006). https://doi.org/10.1103/PhysRevB.73.193306
10. M. Klaas, H. Flayac, M. Amthor et al., Phys. Rev. Lett. **120**, 017401 (2018). https://doi.org/10.1103/physrevlett.120.017401
11. S.S. Demirchyan, T.A. Khudaĭberganov, I.Yu. Chestnov and A. P. Alodzhants, J. Opt. Technol. **84**, 75 (2017). https://doi.org/10.1364/jot.84.000075
12. P.D. Drummond, C.W. Gardiner, Phys. A Math. Gen. **13**, 2353–2368 (1980). https://doi.org/10.1088/0305-4470/13/7/018
13. P.D. Drummond, K.J. McNeil, D.F. Walls, Opt. Acta Int. J. Opt. **321**, 27 (1980). https://doi.org/10.1080/713820226
14. H. Jabri, Phys. Rev. A **101**, 053819 (2020). https://doi.org/10.1103/PhysRevA.101.053819
15. F. Zou, D.-G. Lai, J.-Q. Liao, Opt. Express **28**, 16175–16190 (2020). https://doi.org/10.1364/OE.391628
16. A.V. Yulin, O.A. Egorov, F. Lederer, D.V. Skryabin, Phys. Rev. A **78**, 061801061801 (2008). https://doi.org/10.1103/PhysRevA.78.061801
17. C. Gardiner, *Stochastic Methods: a Handbook for the Natural and Social Sciences*, 4th edn. (Springer, Berlin, 2009). (**ISBN 978-3-540-70712-7**)
18. H. Haken, *Synergetics: Introduction and Advanced Topics* (Springer Science & Business Media, New York, 2013). (**ISBN 978-3-662-10184-1**)
19. W. Casteels, F. Storme, A. Le Boité, C. Ciuti, Phys. Rev. A **93**, 033824 (2016). https://doi.org/10.1103/PhysRevA.93.033824
20. W. Casteels, R. Fazio, C. Ciuti, Phys. Rev. A **95**, 012128 (2017). https://doi.org/10.1103/PhysRevA.95.012128
21. Th.K. Mavrogordatos, EPL **116**, 54001 (2016). https://doi.org/10.1209/0295-5075/116/54001
22. E. Zubizarreta Casalengua, J.C. López Carreño, F.P. Laussy, E. del Valle, Laser Photonics Rev. **14**, 1900279 (2020). https://doi.org/10.1002/lpor.201900279
23. A. Delteil, T. Fink, A. Schade et al., Nat. Mater. **18**, 219–222 (2019). https://doi.org/10.1038/s41563-019-0282-y
24. L. Mandel, Opt. Lett. **4**(7), 205–207 (1979). https://doi.org/10.1364/OL.4.000205
25. Albrecht Werner, Oleg A.. Egorov, Falk Lederer, Phys. Rev. B **89**, 245307 (2014). https://doi.org/10.1103/physrevb.89.245307
26. T. Khudaiberganov, S. Arakelian, I.O.P. Conf, Ser. Mater. Sci. Eng. **896**, 012126 (2020). https://doi.org/10.1088/1757-899X/896/1/012126
27. G. Muñoz-Matutano, A. Wood, M. Johnsson et al., Nat. Mater. **18**, 213–218 (2019). https://doi.org/10.1038/s41563-019-0281-z
28. K.V. Kheruntsyan, J. Opt. B Quantum Semiclass. Opt. **1**, 225 (1999). https://doi.org/10.1088/1464-4266/1/2/005
29. E.T. Whittaker, G.N. Watson, *A Course of Modern Analysis*, 4th edn. (Cambridge University Press, Cambridge, 2013). (**ISBN 978-0-511-60875-9**)
30. G.N. Watson, *A Treatise on the Theory of Bessel Functions*, 2nd edn. (Cambridge University Press, Cambridge, 1995). (**ISBN 0-521-48391-3**)